Exploiting Material Properties to Select a Suitable Wavelet Basis for Efficient Rendering

Jeroen Put, Nick Michiels and Philippe Bekaert

Hasselt University - tUL - iMinds, Expertise Centre for Digital Media, Wetenschapspark 2, 3590 Diepenbeek, Belgium

Keywords: Rendering, Wavelets, Parameterisation, Materials.

Abstract: Nearly-orthogonal spherical wavelet bases can be used to perform rendering at higher quality and with significantly less coefficients for certain spherical functions, e.g. BRDF data. This basis avoids parameterisation artifacts from previous 2D methods, while at the same time retaining high-frequency details in the lighting. This paper demonstrates the efficiency of this representation for rendering purposes. Regular 2D Haar wavelets can still occasionally perform better, however. This is due to their property of being fully orthogonal. An important novelty of this paper lies in the introduction of a technique to select an appropriate wavelet basis on-the-fly, by utilising prior knowledge of materials in the scene. To show the influence of different bases on rendering quality, we perform a comparison of their parameterisation error and the compression performance.

1 INTRODUCTION

Research in computer graphics has led to mathematical models and algorithms to render photorealistic images (Dutré et al., 2006). A challenging aspect of rendering algorithms is how to parameterise the functions that are used in the rendering equation (Kajiya, 1986). For instance, in an all-frequency relighting framework, it is particularly important to represent all the details in the visibility, BRDF and lighting functions. Previous approaches use harmonic analysis to approximate the lighting, but fail to capture sharp details like shadows and specular highlights. To provide these, representations based on 2D wavelets have been introduced. These representations suffer from distortion artifacts, because a completely uniform one-to-one mapping of the spherical to the planar domain is not available. Their inherent compactness is particulary important for inverse rendering applications, since the estimation of geometry, lighting and material from a set of uncalibrated images is a challenging problem and requires a lot of processing power and storage.

Earlier work focused either on improving the efficiency of the underlying representation or enhancing the performance of triple product calculations. Our contribution in this paper is the combination of these ideas. The nearly-orthogonal basis avoids parameterisation artifacts, while at the same time retaining high-frequency details in the lighting. On the other hand, Ng.'s triple product (Ng et al., 2004) provides an efficient manner to simulate complex lighting interaction from precalculated datasets. It is through the combination of precisely these ideas that we are able to perform rendering with more complex spatially varying BRDFs and more intricate lighting. Another contribution of this paper is the exploitation of prior knowledge of scene materials to choose an appropriate wavelet basis. We have observed during our experiments that specular and diffuse BRDFs require different bases for optimal approximation.

2 PREVIOUS WORK

Rendering requires the processing of vast quantities of data. Often such data consists of visibility, BRDF and lighting information. An efficient representation is required for rendering with high quality and performance. We focus on inverse rendering as an application in this paper, as the problem of large volumes of data is even more pronounced for this category of techniques. Earlier techniques used spherical harmonics, extending Fourier decomposition to the spherical domain (Okabe et al., 2004; Yu et al., 2006). Spherical harmonics have the disadvantage that they can only represent low frequencies. For high frequencies, the number of coefficients required grows exponentially. This makes solving the triple product (Ng et al., 2004) integral inefficient. Okabe et al. (Ok-
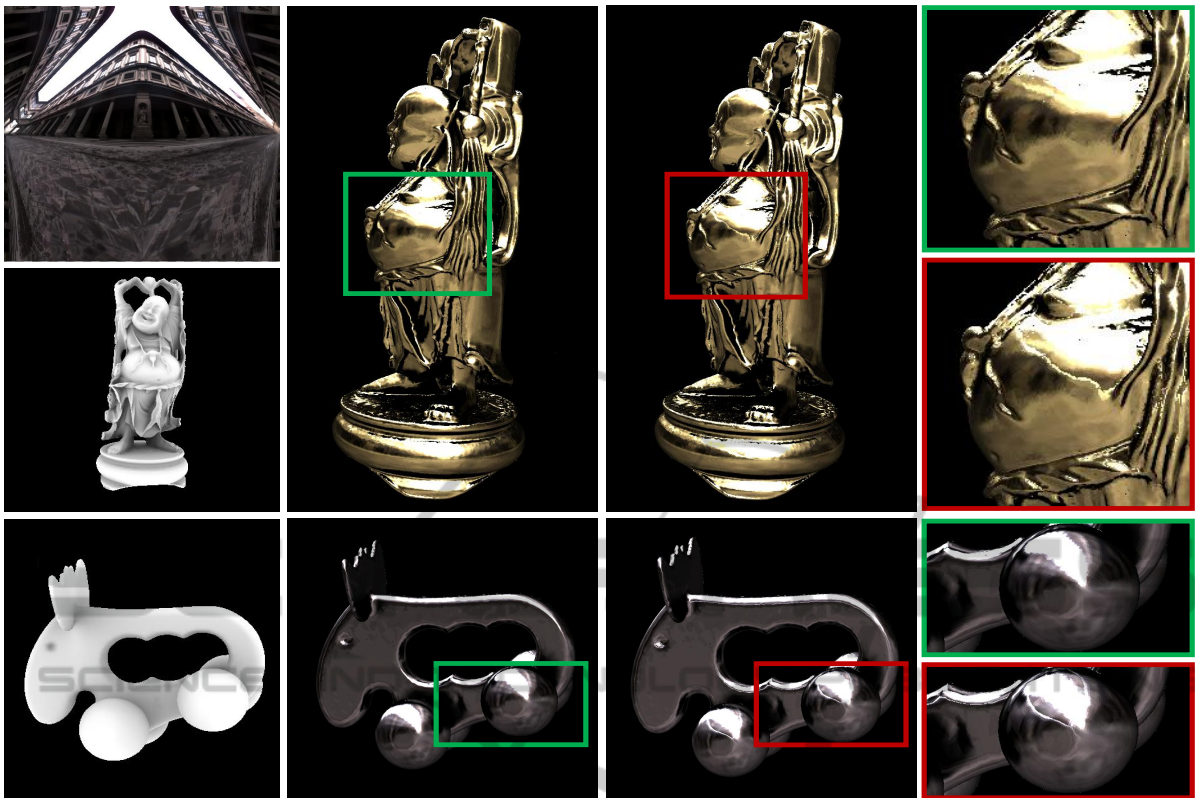
Figure 1: Quality comparison for two different datasets. Leftmost column: environment map and meshes. Two central columns: Rendering with optimal choice of basis (green) versus 2D parameterisation (red). Rightmost column: Zoomed images to compare quality. Our method reduces parameterisation errors. See also the video accompanying this paper.

abe et al., 2004) showed an alternative representation based on 2D Haar wavelets. Haber et al. (Haber et al., 2009) use a 2D Haar wavelet basis to represent the BRDF and visibility functions for every vertex in the scene and to approximate the illumination environment map for every viewpoint. The main advantage is that 2D Haar wavelets are able to capture high frequency detail. However, they also suffer the disadvantage that there is no one-to-one mapping from the planar domain to the spherical domain, resulting in distortion when using 2D wavelets to represent spherical functions. To minimise the distortion, octahedral parametrisation (Praun and Hoppe, 2003a) is often used.

Sweldens et al. (Schröder and Sweldens, 1995) proposed the construction of various wavelet basis functions on the surface of the sphere. This construction is based on his earlier work on the lifting scheme. He concluded that lifted spherical wavelets are particulary performant for the representation of BRDF functions. This paper draws from these ideas, but contributes by combining the triple product integration from Ng. (Ng et al., 2004) with a nearly-orthogonal wavelet basis.

A large body of work has been dedicated to the analysis and representation of BRDFs (Ruiters and Klein, 2010; Bilgili et al., 2011). However, these representations are not particularly suitable for other spherical functions, such as the illumination. Tsai et al (Tsai et al., 2008) developed an importance sampling strategy to sample products from illumination and BRDF with spherical radial basis functions. This technique is limited in its application, due to the costly process of fitting their basis functions. Their method also focuses on double products, where we require triple product integral calculations in our forward rendering.

The remainder of this paper is organized as follows. Section 3 shows how a Haar wavelet basis can be constructed on a sphere and explains which subdivision scheme is required. Section 4 presents the results, where a comparison is made between the new spherical Haar wavelet basis and the original 2D Haar wavelet basis. Finally we complete this paper by presenting our conclusions and future work in Section 5.

3 SPHERICAL HAAR WAVELETS

Many functions in graphics are naturally expressed in the spherical domain. Like previous methods, in our rendering application the light at every surface point x is expressed as a triple product integral:

$$B(x, \omega_0) = \int_\Omega L(x, \omega_i) V(x, \omega_i) \rho(x, \omega_i, \omega_o)(\omega_i \cdot n(x)) d\omega_i \tag{1}$$

In this equation, B is the radiance as a function of position x and outgoing direction ω_o. L and V are the lighting and visibility functions respectively, ρ is the BRDF and n is the surface normal. To avoid the need for separate environment maps per vertex, we assume furthermore that L is a distant illumination function and incorporate the term $(\omega_i \cdot n(x))$ into V, so equation 1 becomes:

$$B(x, \omega_0) = \int_\Omega \tilde{L}(\omega_i) V(x, \omega_i) \rho(x, \omega_i, \omega_o) d\omega_i \tag{2}$$

L, V and ρ are all functions on the spherical domain Ω. $\tilde{L}$ is the globally defined environment map, rotated into the local frame of V and ρ.

Current techniques use 2D Haar wavelets and are able to represent details with relatively few coefficients. On the other hand, they introduce distortion artifacts due to the parameterisation step of the spherical domain to the planar domain. Often, the hemi-octahedral parameterisation by Praun and Hoppe is used to perform this mapping (Praun and Hoppe, 2003b):

$$V(\omega) = \sum_i V_i \Psi_i(\omega),$$
$$\tilde{L}(\omega) = \sum_j \tilde{L}_j \Psi_j(\omega), \tag{3}$$
$$\rho(\vec{x}, \omega) = \sum_k \rho_k(\vec{x}) \Psi_k(\omega)$$

where Ψ is an appropriate basis on the octahedron. In this paper, V, ρ and L are projected into a spherical wavelet basis Ψ. This way, we can write equation 2 in terms of these basis functions:

$$B(x, \omega_0) = \sum_i \sum_j \sum_k L_i V_j \rho_k \int_\Omega \Psi_i(\omega) \Psi_j(\omega) \Psi_k(\omega) d\omega \tag{4}$$

$\Psi_i(\omega)$, $\Psi_j(\omega)$ and $\Psi_k(\omega)$ are the tripling coefficients, as defined by Ren et al. (Ng et al., 2004). More recent work pointed out the existence of a generalized wavelet product integral (Sun and Mukherjee, 2006).

3.1 Wavelet Basis and Subdivision Scheme

To avoid artifacts, sampling of the spherical function domain should happen as uniform as possible. In this paper, an octahedral subdivision structure was chosen, because of its favourable sampling characteristics and because of symmetric sampling of hemispheric functions.

The wavelet basis is defined over the triangles of the subdivision scheme. Each of the octahedron octants is represented by a quadtree of wavelet coefficients. In each subdivision step, every triangle is split into four children, using the geodesic bisector criterium as defined by Sweldens et al. (Schröder and Sweldens, 1995).

Let T^k be such a triangle at depth k (k=0 for the lowest level). T_0^{k+1}, T_1^{k+1}, T_2^{k+1} and T_0^{k+1} are the four children of T^k. Figure 2 shows an example of such a triangle.

Figure 2: Decomposition of four pixel values into one scaling coefficient and three wavelet coefficients (Bonneau, 1999).

Here, Φ^k represents a scaling function. It is a constant function with value 1 on T^k and zero otherwise. Ψ_1^k, Ψ_2^k and Ψ_3^k are the three wavelet functions, with T^k as their support.

A fundamental property of the above triangular Haar wavelets, is that every piecewise constant function over the four subtriangles ($T^{K+i}, i = 0, 1, 2, 3$) can be expressed as a linear combination of the constant scaling function and the three wavelet functions. From this, a local reconstruction can be derived, which converts this combination of functions to colour values again. The conversion of a scaling function and three wavelet functions into colour values is called synthesis:

$$\begin{bmatrix} x_0^{k+1} \\ x_1^{k+1} \\ x_2^{k+1} \\ x_3^{k+1} \end{bmatrix} = \begin{bmatrix} 1 & r_{01}^k & r_{02}^k & r_{03}^k \\ 1 & r_{11}^k & r_{12}^k & r_{13}^k \\ 1 & r_{21}^k & r_{22}^k & r_{23}^k \\ 1 & r_{31}^k & r_{32}^k & r_{33}^k \end{bmatrix} \begin{bmatrix} x^k \\ y_1^k \\ y_2^k \\ y_3^k \end{bmatrix} \tag{5}$$

Here, r_{ij}^k is the value of ψ_j^k for the subtriangle T_i^{k+1}. Analysis can be performed by inverting the foregoing synthesis matrix.

Figure 3: Compression with Bonneau spherical wavelets. Left: original; Right: reconstruction with 5% of the coefficients.

3.2 Choosing a Suitable Basis

During our evaluation, we experimented with various Haar wavelet bases. The first representation were the Bio-Haar wavelets introduced by Sweldens et al. (Schröder and Sweldens, 1995). This basis has the property of being semi-orthogonal:

$$\int \psi_1^k \phi^k = \int \psi_2^k \phi^k = \int \psi_3^k \phi^k = 0 \qquad (6)$$

Semi-orthogonality is a necessary condition for the existence of a wavelet basis over a certain domain. This paper has opted for the nearly-orthogonal Bonneau wavelet basis (Bonneau, 1999). This basis is, in the limit of its subdivision, guaranteed to provide good compression performance when truncating the least significant coefficients. At the same time it is a convenient basis for a triple product integral implementation. Figure 3 demonstrates the compression on a spherical image.

More interesting bases, like SOHO wavelets (Lessig, 2007), also provide orthogonality:

$$\int \psi_1^k \psi_2^k = \int \psi_1^k \psi_3^k = \int \psi_2^k \psi_3^k = 0 \qquad (7)$$

Orthogonality guarantees that the best approximation of the L_2-norm can be achieved when removing the least significant coefficients. They also have the advantage of a fast matrix inversion for the analysis stage. SOHO wavelets provide orthogonality, but do so at the cost of increased computation for their subdivision scheme to create triangles of equal area, while not providing upper bounds on the distortion of image quality of this scheme.
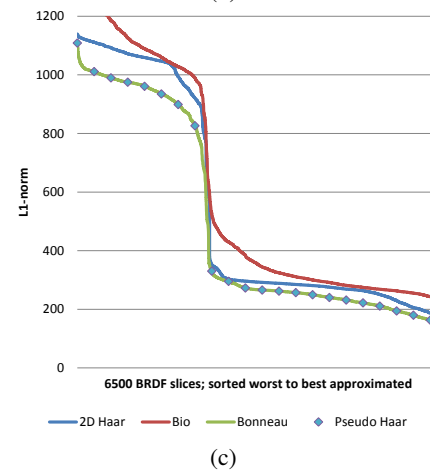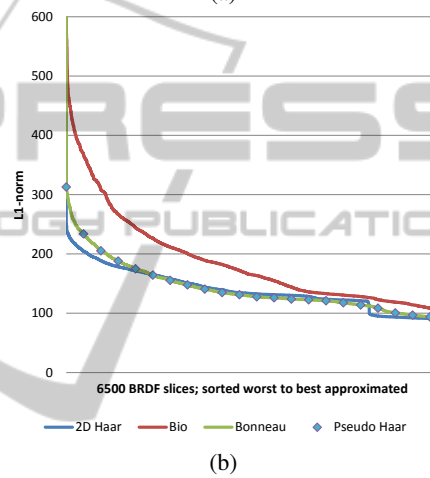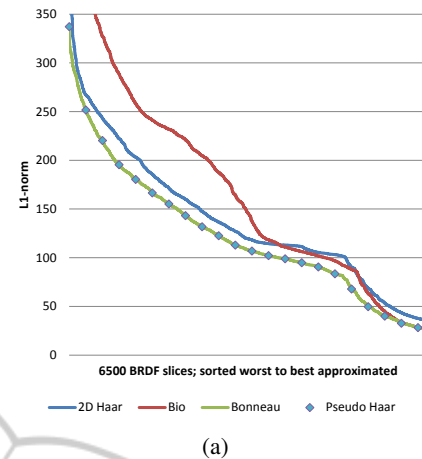

(a)

(b)

(c)

Figure 4: Comparison of compression performance in the L_1-norm of four wavelet bases on a database with (a) a representative mixture of BRDF slices, (b) more specular BRDF slices and (c) more diffuse BRDF slices. 5% of coefficients were retained. A smaller norm is better. Our application chooses the best basis on-the-fly, by taking the material properties into account. As a consequence we always get the best possible representation.
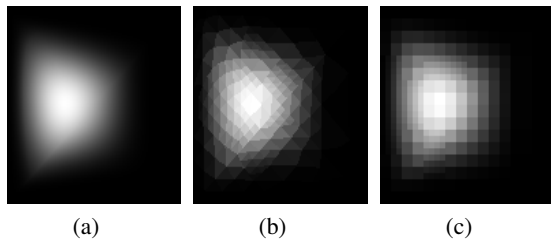
Figure 5: Comparison of a diffuse BRDF approximation. 2% of coefficients retained. Smaller L_2-norm is better. (a) original; (b) spherical wavelets (L_2-norm: 2,2739); (c) 2D Haar-wavelets (L_2-norm: 2,5831).
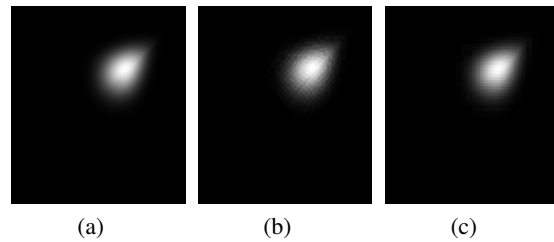

Figure 6: Comparison of specular BRDF approximation. 2% of coefficients retained. Smaller L_2-norm is better. (a) original; (b) spherical wavelets (L_2-norm: 0,9323); (c) 2D Haar-wavelets (L_2-norm: 0,8895).

4 RESULTS

This section will compare the performance and quality of the nearly-orthogonal spherical wavelet representation in a rendering context. Good compression performance guarantees the need for less coefficients. Therefore, this shall be the main focus in this section.

Figure 4 shows a comparison of compression performance of five wavelet bases in the L_1-norm on a database of BRDF functions. In literature, it is argued that the L_1-norm often corresponds better to the visual perception by humans observers (Antonini et al., 1992). The five wavelet bases are the lifted Bio-Haar basis introduced by Sweldens et al. (Schröder and Sweldens, 1995), the regular 2D Haar wavelets used by Haber et al. (Haber et al., 2009), the pseudo Haar spherical wavelet basis suggested by Ma et al. (Ma et al., 2006) and the two nearly-orthogonal Bonneau spherical wavelets (Bonneau, 1999). We do not include a comparison with a spherical harmonics basis, as its unsuitability for representing high frequencies has already been proved in earlier literature (Ng et al., 2004). Every representation performed compression with a fixed budget of coefficients, where the least significant coefficients were truncated. We used the MERL BRDF database (Matusik et al., 2003; Ngan et al., 2005) for rendering since it contains a representative mixture of Lambertian, Cook-Torrance and Lafortune BRDF slices. The chart sorts the BRDF functions from worst to best approximated. It can be observed that the Bio-Haar basis is significantly outperformed in nearly all cases by the other bases. Both Bonneau and pseudo Haar bases have better compression performance than the 2D Haar basis. The pseudo Haar basis performs identical to the Bonneau basis.

To confirm our observation that spherical wavelets compress diffuse BRDF slices better than very specular BRDF slices, we customised the content of the internal BRDF database. This results in two additional graphs. The first graph is displayed in Figure 4(b) and shows a scenario with significantly more specular BRDF slices. The graph shows that the spherical wavelets perform slightly worse than the 2D Haar wavelets. The second graph is shown in Figure 4(c) and demonstrates a scenario with predominantly diffuse BRDF slices. The graph clearly demonstrates that there are two groups of BRDF approximations. The approximation yields large norms for specular BRDFs and lower norms for more diffuse BRDFs. The contents of the database has an influence on how the two groups are distributed on the graph. This indicates that the choice of wavelet basis can significantly enhance the compression performance if prior knowlege of material properties in the scene is available. Therefore the selection of an appropriate basis can be guided by the location of the cut-off that separates the two groups.

For the next part of our evaluation, we select some noteworthy BRDF slices out of the BRDF databse. A BRDF slice is defined as a 2D subfunction of a 6D BRDF defined over the hemisphere of all incomming directions In Figure 5, a comparison of diffuse BRDF slice approximation is shown between the Bonneau spherical wavelet basis and the 2D Haar wavelet basis. It can be seen that the spherical wavelets provide 13,59% better compression performance in this case.

Figure 6 shows another comparison, with a strongly specular BRDF. This time, 2D Haar wavelets outperform spherical wavelets, albeit marginally. This is a trend that was observed during our experiments. We believe this is due to three main factors. First, spherical wavelets approximate the original signal with the triangles of the underlying octahedral subdivision scheme, while 2D Haar wavelets use rectangular areas (pixels). A large portion of specular BRDFs tend to have a circular shape, due to the distribution of light around the specular lobe. It was observed in our implementation that the circular shape can be approximated by fewer coefficients with rectangular areas.

Second, specular BRDFs with a large specular exponent subtend only a small solid angle on the hemi-

sphere. It is therefore less likely that the specular lobe will cross areas of non-uniform sampling due to the parameterisation method. In the cases such specular BRDFs do overlap such areas, they are expected to undergo severe distortion.

Finally, in the aforementioned case where very specular BRDFs avoid parameterisation artifacts, the 2D Haar wavelets are expected to slightly outperform the spherical wavelets. This can be attributed to the fact that the 2D Haar basis is a fully orthogonal basis, while the nearly-orthogonal wavelet bases are only orthogonal in the limit of the subdivision. As demonstrated by Sweldens et al. (Schröder and Sweldens, 1995), BRDF functions can be represented with very few coefficients and the approximation therefore often takes place on a low number of subdivisions of the underlying octahedral structure.

To have a more clear measure of the parameterisation error, independent from different wavelet representations, we performed another experiment shown in Figure 8. Here, we first sampled the BRDF slices uniformly on the unit sphere with a statistical method (Dutré et al., 2006) as a ground truth. We then sampled the same slices with the octahedron as well as with the 2D parameterisation method. Figure 8 shows the accumulated error for both parameterisations in comparison with the ground truth. We can conclude that avoiding parameterisation artifacts yields better quality approximation.

Figure 7 demonstrates the effectiveness of the spherical wavelets for different compression ratios. This graph can be used to read the reduction in coefficients for a certain norm. For example in Figure 7(a), to reach an L_1-norm of 20, the sperical wavelets use 9% less coefficients. A first observation is that for a relatively diffuse BRDF, as shown in (a), the spherical wavelet outperforms the 2D Haar wavelet over all compression ratios. Second, for a more specular BRDF, as shown in (b), both wavelets perform equally well. If we perform this experiment on the entire BRDF database, spherical wavelets require on average 20% less coefficients. In the best case we observed 40% reduction in coefficients. A comparison between our basis selection algorithm and regular 2D parameterisation is shown in Figure 1.

5 CONCLUSIONS

This paper has introduced the use of nearly-orthogonal spherical wavelets to perform rendering at higher quality and lower computational cost. Our evaluation shows that spherical wavelets often outperform 2D Haar wavelets, because they avoid inherent
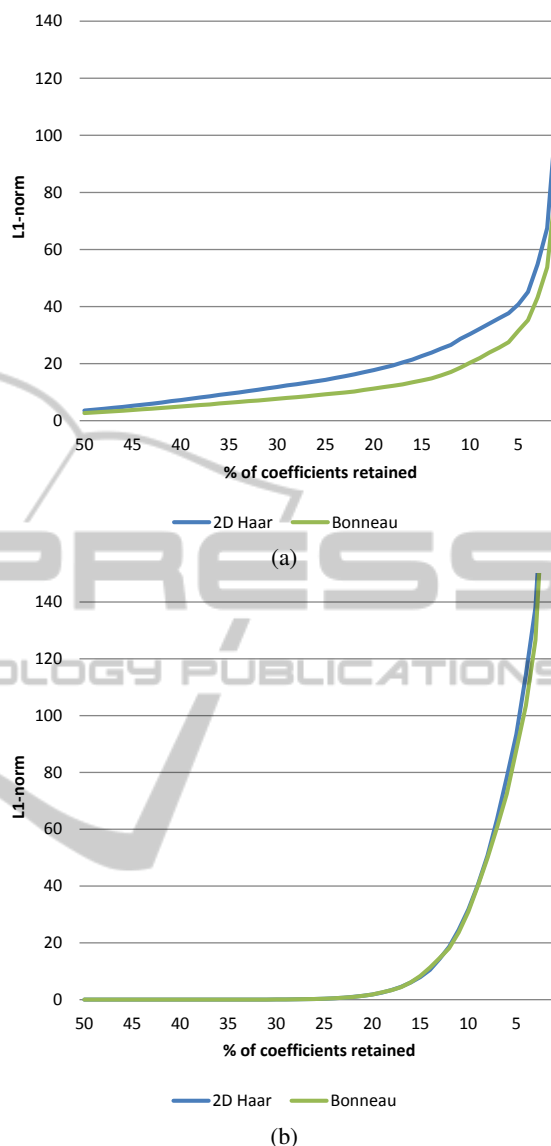

(a)

(b)

Figure 7: Wavelet performance for different compression ratios: (a) almost diffuse BRDF; (b) specular BRDF. It is shown that material properties are a good indicator for an on-the-fly choice of compression ration.

parameterisation errors. By utilising prior knowledge of scene materials, we can adaptively choose an appropriate wavelet based on a specularity criterium. Separation of materials in diffuse and specular provides only a rough categorisation, but in practise we observed that compression performance of spherical versus 2D Haar wavelets is strongly linked with these properties.
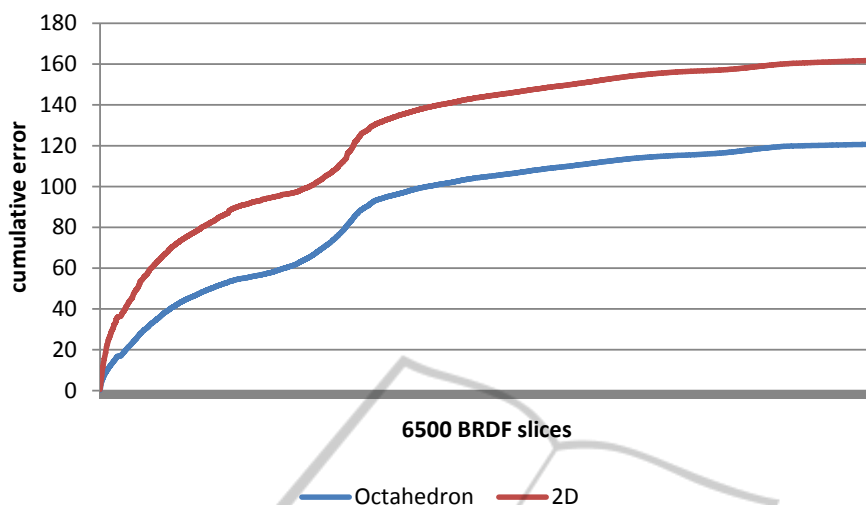
Figure 8: Cumulative parameterisation error compared to the ground truth. Octahedron (spherical) parameterisation outperforms regular 2D parameterisation.

ACKNOWLEDGEMENTS

REFERENCES

Antonini, M., Barlaud, M., Mathieu, P., and Daubechies, I. (1992). Image coding using wavelet transform. *IEEE Transactions on Image Processing*, 1(2):205–220.

Bilgili, A., Öztürk, A., and Kurt, M. (2011). A general brdf representation based on tensor decomposition. *Comput. Graph. Forum*, 30(8):2427–2439.

Bonneau, G.-P. (1999). Optimal triangular haar bases for spherical data. *LMC - CRNS*.

Dutré, P., Bala, K., and Bekaert, P. (2006). *Advanced global illumination, 2nd edition*. A K Peters (http://www.akpeters.com/).

Haber, T., Fuchs, C., Bekaert, P., Seidel, H.-P., Goesele, M., and Lensch, H. P. A. (2009). Relighting objects from image collections.

Kajiya, J. T. (1986). The rendering equation. In *Proceedings of the 13th annual conference on Computer graphics and interactive techniques*, SIGGRAPH '86, pages 143–150, New York, NY, USA. ACM.

Lessig, C. (2007). Orthogonal and symmetric haar wavelets on the sphere. *Master thesis - University of Toronto*.

Ma, W.-C., Hsiao, C.-T., Lee, K.-Y., Chuang, Y.-Y., and Chen, B.-Y. (2006). Real-time triple product relighting using spherical local-frame parameterization. *Vis. Comput.*, 22(9):682–692.

Matusik, W., Pfister, H., Brand, M., and McMillan, L. (2003). A data-driven reflectance model. *ACM Transactions on Graphics*, 22(3):759–769.

Ng, R., Ramamoorthi, R., and Hanrahan, P. (2004). Triple product wavelet integrals for all-frequency relighting. *ACM Trans. Graph.*, 23(3):477–487.

Ngan, A., Durand, F., and Matusik, W. (2005). Experimental analysis of brdf models. In *Proceedings of the Sixteenth Eurographics conference on Rendering Techniques*, EGSR'05, pages 117–126, Aire-la-Ville, Switzerland, Switzerland. Eurographics Association.

Okabe, T., Sato, I., and Sato, Y. (2004). Spherical harmonics vs. haar wavelets: Basis for recovering illumination from cast shadows. In *Shadows, Proc. Conf. Computer Vision and Pattern Recognition*, pages 50–57.

Praun, E. and Hoppe, H. (2003a). Spherical parametrization and remeshing. *ACM Trans. Graph.*, 22(3):340–349.

Praun, E. and Hoppe, H. (2003b). Spherical parametrization and remeshing. *ACM TOG*, 22(3):340–349.

Ruiters, R. and Klein, R. (2010). A compact and editable representation for measured brdfs. Technical Report CG-2010-1, University of Bonn.

Schröder, P. and Sweldens, W. (1995). Spherical wavelets: Efficiently representing functions on the sphere. *University of South Carolina*.

Sun, W. and Mukherjee, A. (2006). Generalized wavelet product integral for rendering dynamic glossy objects. In *ACM SIGGRAPH 2006 Papers*, SIGGRAPH '06, pages 955–966, New York, NY, USA. ACM.

Tsai, Y.-T., Chang, C.-C., Jiang, Q.-Z., and Weng, S.-C. (2008). Importance sampling of products from illumination and brdf using spherical radial basis functions. *The Visual Computer*, 24(7-9):817–826.

Yu, T., Wang, H., Ahuja, N., and Chen, W.-C. (2006). Sparse lumigraph relighting by illumination and reflectance estimation from multi-view images. In *ACM SIGGRAPH 2006 Sketches*, SIGGRAPH '06, New York, NY, USA. ACM.